nanomaterials

MDPI

Article

Positron Annihilation Lifetime Spectroscopy Insight on Free Volume Conversion of Nanostructured $MgAl_2O_4$ Ceramics

Halyna Klym [1,*], Ivan Karbovnyk [1,2], Sergei Piskunov [3] and Anatoli I. Popov [3,*]

[1] Specialized Computer Systems Department, Lviv Polytechnic National University, 12 Bandera Str., 79013 Lviv, Ukraine; ivan_karbovnyck@yahoo.com
[2] Department of Electronics and Computer Technologies, Ivan Franko National University of Lviv, 50 Dragomanov Str., 79005 Lviv, Ukraine
[3] Institute for Solid State Physics, University of Latvia, Kengaraga 8, LV-1063 Riga, Latvia; sergejs.piskunovs@lu.lv
* Correspondence: halyna.i.klym@lpnu.ua (H.K.); popov@latnet.lv (A.I.P.)

Abstract: Herein we demonstrate the specifics of using the positron annihilation lifetime spectroscopy (PALS) method for the study of free volume changes in functional ceramic materials. Choosing technological modification of nanostructured $MgAl_2O_4$ spinel as an example, we show that for ceramics with well-developed porosity positron annihilation is revealed through two channels: positron trapping channel and ortho-positronium decay. Positron trapping in free-volume defects is described by the second component of spectra and ortho-positronium decay process by single or multiple components, depending on how well porosity is developed and on the experimental configuration. When using proposed positron annihilation lifetime spectroscopy approaches, three components are the most suitable fit in the case of $MgAl_2O_4$ ceramics. In the analysis of the second component, it is shown that technological modification (increasing sintering temperature) leads to volume shrinking and decreases the number of defect-related voids. This process is also accompanied by the decrease of the size of nanopores (described by the third component), while the overall number of nanopores is not affected. The approach to the analysis of positron annihilation lifetime spectra presented here can be applied to a wide range of functional nanomaterials with pronounced porosity.

Keywords: nanostructured ceramics; positron annihilation; positronium decay; positron trapping; free-volume defects; nanopores

Citation: Klym, H.; Karbovnyk, I.; Piskunov, S.; Popov, A.I. Positron Annihilation Lifetime Spectroscopy Insight on Free Volume Conversion of Nanostructured $MgAl_2O_4$ Ceramics. *Nanomaterials* **2021**, *11*, 3373. https://doi.org/10.3390/nano11123373

Academic Editor: Graeme Watson

Received: 18 October 2021
Accepted: 10 December 2021
Published: 13 December 2021

1. Introduction

Positron annihilation lifetime spectroscopy (PALS) technique is considered as one of the promising alternative methods to analyze free volume and defects in functional and other materials [1–5], including ceramics [6–8], glasses [9–11], polymers [12–14], nanocomposites [15–17], etc. There are already several attempts to develop a phenomenological model describing the processes of positron annihilation in metal powders that contain Cu-, W-, Ni- [18], some types of $BaTiO_3$ [19–21] and $SrTiO_3$ perovskites [22,23], nanocrystallite ferrites [24,25], Ni–Cr alloy [26], In_2O_3 nanocrystals [27], irradiated W and Fe [28], water diffusivity transition in composites [29,30] and others. Different approaches to the analysis of annihilation spectra as well as decompositions with a different number of components were introduced. It was shown that the main positron annihilation channels in these materials can be related to positron trapping and ortho-positronium (o-Ps) decay. The best results were achieved when using the decomposition involving three independent components [31–33]. In the frame of this model, the second component describes capturing of positrons by free volume defects such as vacancy clusters, neutral surfaces of powder particles, or vacancies with a negative charge, particularly those that are close to grain boundaries. The shortest component is related to the annihilation of the defect-free mass

with slight mixing with other positron trapping channels and para-positronium (p-Ps). The longest third component corresponds to ortho-positronium (o-Ps) atoms decay [34].

Earlier, we have carried out PALS investigations aimed at exploring free volume changes in Ge-Ga-S(Se) chalcogenide glasses under thermal influences [35], compositional modification (in particular, CsCl addition) and during crystallization processes [36–39]. Additionally, the investigation of moisture adsorption processes on the free volume changes in $MgAl_2O_4$ ceramics was carried out [25,40,41]. For each of mentioned functional materials, the appropriate models of positron annihilation were suggested, assuming two, three- or four-component decomposition depending on the structural peculiarities. The approach to PALS analysis that allows estimating the influence of additional modifiers on the free volume change was also proposed [38]. However, for most of the mentioned approaches, the initial analysis is often significantly complicated.

The goal of this work is to present a universal approach that can be used to study free volume in functional ceramic materials with pronounced porosity.

The approach is explained in the example of $MgAl_2O_4$ spinel ceramics. $MgAl_2O_4$ ceramics are characterized by developed grain structure, grain boundaries, and pores. Change of the free volume in this material due to technological modification can be considered a model example for a study by means of PALS. A demonstrated approach to the decomposition and the analysis of annihilation spectra of ceramics should allow the application of the technique in the case of other functional nanoporous materials.

2. Materials and Methods

$MgAl_2O_4$ ceramics understudy was obtained from initial MgO powders with the specific surface of 10.7 ± 2 m^2/g and Al_2O_3 powders with the specific surface of 12.4 ± 2 m^2/g, taken in 1:1 molecular ratio. To modify the ceramics, the highest temperatures of isothermal sintering were used (1100 °C, 1200 °C, 1300 °C, and 1400 °C) and sintering durations were set to 2 h, 5 h, and 9 h. In greater detail, the technology of $MgAl_2O_4$ ceramics preparation is described in [41,42].

According to the results of X-ray diffraction [42], ceramics sintered at 1100–1200 °C during 2 h exhibits reflexes of three phases: along with the principal $MgAl_2O_4$ spinel phase, there are MgO (11.25% for the ceramics sintered at 1100 °C and 5.82% for the ceramics sintered at 1200 °C) and Al_2O_3 (8.13% for the ceramics sintered at 1100 °C and 6.06% for the ceramics sintered at 1200 °C) phases. Ceramics sintered at 1300 °C and 1400 °C temperatures during 2 h show only reflexes of the single additional phase MgO in the amount of 3.5 and 1.5%, respectively. Similar values were observed for ceramics sintered during 5 and 9 h.

Evolution of free volume in $MgAl_2O_4$ ceramics was experimentally studied by PALS method using ORTEC spectrometer (with conventional fast-fast coincidence system of 270 ps resolution, full width at half maximum FWHM of a single Gaussian, determined by 60Co isotope measuring) at the temperature T = 22 °C and relative humidity RH = 35% [43,44]. For each pair of samples under study, three spectra of PALS were collected. The difference between these spectra was in the number of ordinary annihilation events that were in the range of 800,000 to 1,200,000. Each spectrum was subjected to multiple processing by the LT program due to small changes in the number of final channels, annihilation background, and the time shift of the spectrum. The best results were selected based on the least-squares fit between experimental points and theoretical curve [45]:

$$FIT = \frac{\sum_{k=1}^{N}\left(\frac{T_k - E_k}{\sqrt{E_k}}\right)^2}{N-m} \approx \frac{1}{N}\sum_{k=1}^{N}\left(\frac{T_k - E_k}{\sqrt{E_k}}\right)^2, \quad (1)$$

where N is the number of channels (or the number of experimental points), E_k–measured counts in the k-th channel, T_k–theoretical counts in the k-th channel, $\sqrt{E_k}$–mean square deviation of counts in the k-th channel and m is the number of fitting parameters. The

value T_k is selected automatically in the LT program depending on the selected model, which best describes the theoretical curve.

As a result, several data groups having a different number of experimental points N were formed within the selected fitting procedure. Only results with FIT values close to 1 (optimal deviation was in the range from 0.95 to 1.2) were considered as optimal ones within the chosen model. In the next step, these values and determined PALS characteristics were controlled depending on the annihilation background and time shift of the PALS spectrum, the results show only minor changes selected by us. It should be noted that the source correction and spectrometer resolution function remained unchanged in the above algorithm.

Since low statistic measurement mode was exploited, spectra were decomposed into three components by means of LT software (version 10.2.2) [46]. Best results selection was done in steps. First, results with FIT exceeding 1.2 were dropped. Second, groups with close FIT values in increasing order were formed and results with various values of lifetimes within one group were ignored. Third, for preliminary assessment, average positron lifetimes were calculated for each group. Next, FIT values, lifetimes, and intensities were averaged for each group. Ultimately, the best results with minimum FIT values were chosen and used for further analysis.

By processing the PALS spectra by the LT program, it is possible to obtain the values of the fitting parameters, i.e., lifetimes and intensities with an accuracy of ±0.001 ns and ±0.1%, respectively. However, given that the accuracy of lifetime measurements using the ORTEC spectrometer, in this case, is ±0.01 ns, the lifetimes obtained in the process of mathematical adjustment and the intensities of the respective components were rounded to 0.01 ns and 0.01 a.u. (or 1%), respectively.

3. Results and Discussion

As shown in [41,44], the best results of PALS spectra processing in LT software for $MgAl_2O_4$ ceramics can be achieved with the three-component fitting procedure (in the case of low statistic measurement mode). Therefore, this approach was applied for the analysis of extended positron-trapping defects and nanopores in technologically modified ceramics sintered at 1100–1400 °C during 2, 5, and 9 h.

PALS spectra for $MgAl_2O_4$ ceramics sintered at 1100–1400 °C during 2 h with three components decomposition for ceramics sintered at 1400 °C are shown in Figure 1.

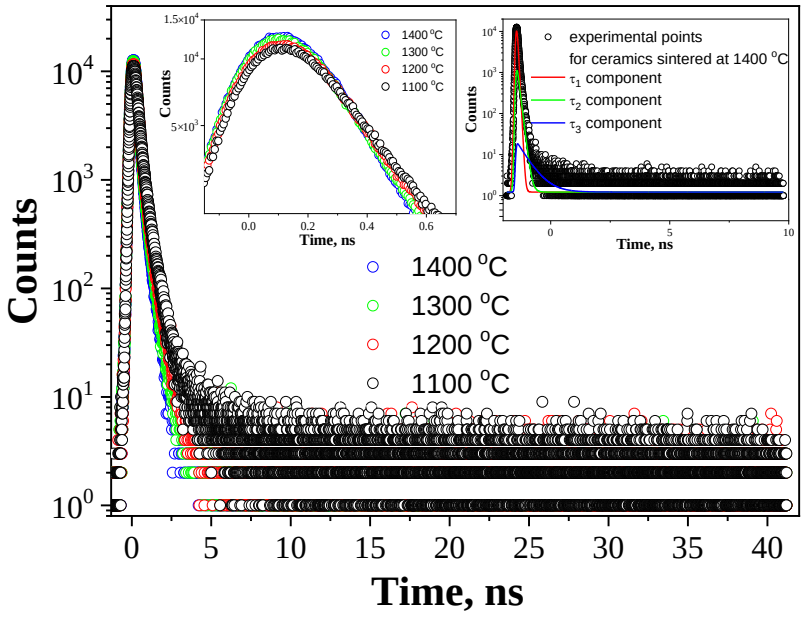

Figure 1. PALS spectra for $MgAl_2O_4$ ceramics sintered at 1100–1400 °C for 2 h with three components decomposition curves for ceramics sintered at 1400 °C.

Typical spectra for ceramics are characterized by a narrow peak and long smooth decay region, where counts are decreased with time. Mathematical three-component decomposition is represented by the sum of exponential decay functions with different powers inversely proportional to the positron lifetimes τ_1, τ_2, and τ_3. The areas under each curve are proportional to intensities I_1, I_2, and I_3.

Besides the main fitting parameters (positron lifetimes τ_1, τ_2 and τ_3 and intensities I_1, I_2, and I_3) that are acquired directly in LT software, the average positron lifetime τ_{av} that reflects the properties of the prevailing defect environment in the material was calculated using two-state positron trapping model [45]:

$$\tau_{av.} = \frac{\tau_1 I_1 + \tau_2 I_2}{I_1 + I_2}. \quad (2)$$

We have also estimated the lifetime τ_b related to the annihilation of positrons in the defect-free region:

$$\tau_b = \frac{I_1 + I_2}{\frac{I_1}{\tau_1} + \frac{I_2}{\tau_2}}. \quad (3)$$

Trapping rate κ_d at which positrons are captured by defects was calculated as follows:

$$\kappa_d = \frac{I_2}{I_1}\left(\frac{1}{\tau_b} - \frac{1}{\tau_2}\right). \quad (4)$$

For spinel ceramics, the difference $\tau_2 - \tau_b$ is treated as an average size of the defect region where positrons are trapped, while τ_2/τ_b ratio is looked at as the parameter that reflects the nature of volume defects [44].

In [44,46,47] it was shown that for functional ceramic materials two PALS channels are enabled: "free" positron trapping (the component with lifetime τ_2) and o-Ps decaying (component with lifetime τ_3). Within the two-state positron trapping model, the first component with lifetime τ_1 and intensity I_1 includes free annihilation, p-Ps decay and is related also to the positrons' bulk lifetimes τ_b in the samples. For some materials (for example, chalcogenide glasses [35–39]) this component has no physical meaning. In the frame of the proposed unified model [44], in $MgAl_2O_4$ ceramics, the first component with parameters τ_1 and I_1 reflects mainly microstructural specifics of spinel ceramics with characteristic octahedral and tetrahedral vacant cation sites along with a contribution from the annihilation of p-Ps atoms which is not considered in the further analysis. The lifetime τ_2 is related to the size of free-volume defects (voids) near grain boundaries with additional phases and I_2 intensity reflects their amount. The third component (τ_3, I_3) originates from the annihilation of o-Ps atoms in intrinsic nanopores of $MgAl_2O_4$ ceramics.

As can be seen from Figure 2, for nanostructured $MgAl_2O_4$ ceramics obtained at 1100–1400 °C during 2 h, lifetime τ_1 of the first short component is decreasing slightly with increasing T_s, whereas intensity I_1 is growing. Such changes speak in favor of ceramics quality increasing towards higher perfection level when using higher sintering temperatures.

Lifetime of the second component τ_2 is related to the positron trapping in defect-related sites. As known from X-ray diffraction, $MgAl_2O_4$ ceramics contain different amounts of MgO/Al_2O_3 phases [42]. These amounts decrease with increasing T_s. As confirmed by scanning electron microscopy studies [42], additional phases are irregularly distributed across the ceramics volume and are mainly localized near grain boundaries. Separated MgO and Al_2O_3 phases play the role of specific positron trapping centers in the ceramics free volume. Since ceramics obtained at lower temperatures include larger amounts of additional phases, positron trapping in such samples should be more pronounced.

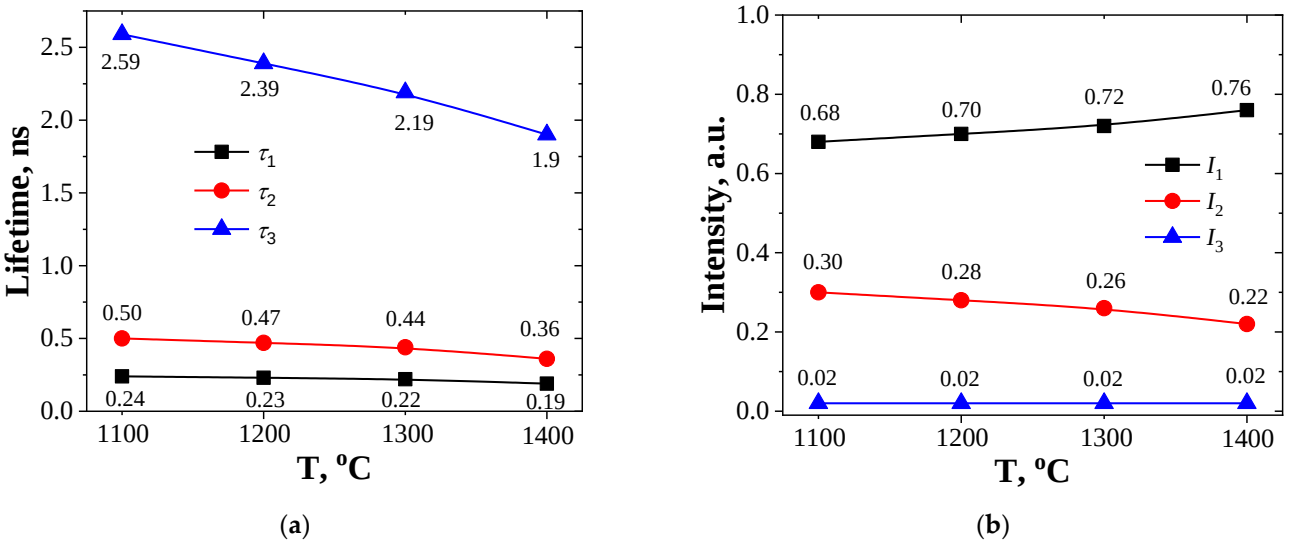

Figure 2. Dependencies of lifetimes (**a**) and intensities (**b**) of the PALS spectrum on the ceramics sintering temperature.

From Figure 2 it also follows that the lifetime and intensity of the second component (τ_2 and I_2, respectively) are essentially decreased with increasing T_s. Lifetime is in correlation with the size of free-volume extended defects (positron trapping center) near grain boundaries and intensity corresponds to the amount of these extended defects. Therefore, with increasing sintering temperature at a fixed 2 h duration one observes the decrease of the free volume where positrons are trapped and the decrease in the number of defects.

Schematically the evolution of the free volume at grain boundaries in the process of the discussed technological modification of $MgAl_2O_4$ ceramics is shown in Figure 3.

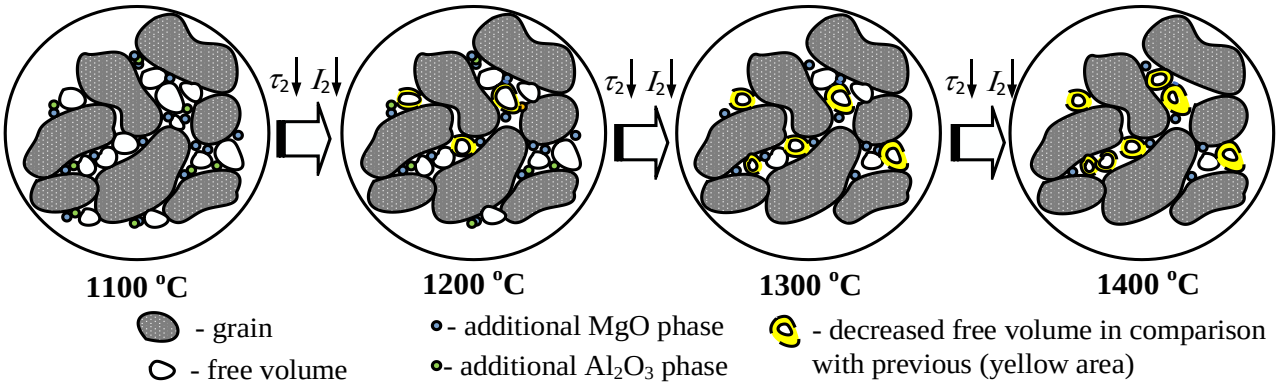

Figure 3. Schematic depiction of the evolution of internal free volume defects at grain boundaries in $MgAl_2O_4$ ceramics.

The third long component of the PALS spectrum (the second channel of positron annihilation with lifetime τ_3 and intensity I_3) is connected to the decay of o-Ps atoms in nanopores and also to the "pick-off" annihilation process [45,48]. As summarized in Figure 2, lifetime τ_3 decreases from 2.59 ns down to 1.9 ns when T_s increases from 1100 °C to 1400 °C. At the same time, intensity I_3 remains unchanged and equals 0.02 a.u. Such behavior indicates the decrease of nanopores size and an unchanged overall number of nanopores. Altogether this means more efficient sintering at higher temperatures. The diagram in Figure 4 further explains the evolution of nanopores near grain boundaries in ceramics.

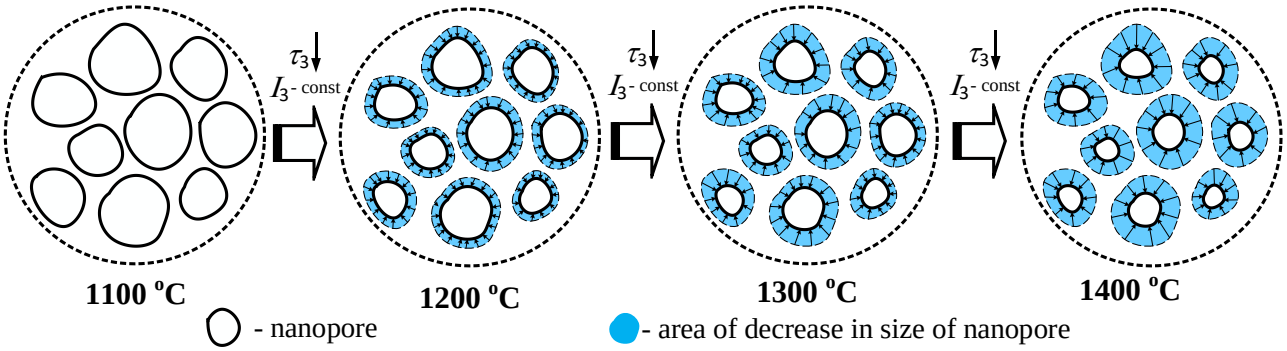

Figure 4. Diagram explaining the evolution of nanopores near grain boundaries in $MgAl_2O_4$ ceramics sintered at 1100–1400 °C during 2 h.

Values of other parameters related to the positron trapping on defects (τ_{av}, τ_b, κ_d) slightly decrease with increasing T_s, which is in fair agreement with the number of additional phases existing in the ceramics understudy near grain boundaries (see Table 1). Even though extended positron trapping defects have an almost identical structural and chemical origin, the value of ($\tau_2 - \tau_b$) is larger in ceramics sintered at lower temperatures. Free-volume geometry (τ_2/τ_b ratio) remains at the level of 1.7. Probably, in these ceramics, the same positron trapping defect center (extended defects near grain boundaries) with a characteristic size of about one-two atomic vacancies prevails, and positron trapping locations have the same nature.

Table 1. Positron trapping parameters and nanopores radii for $MgAl_2O_4$ ceramics sintered at T_s = 1100–1400 °C during 2 h.

T_s, °C	τ_{av}, ns	τ_b, ns	κ_d, ns^{-1}	$\tau_2 - \tau_b$, ns	τ_2/τ_b	R_3, nm
1100	0.32	0.28	0.65	0.21	1.72	0.338
1200	0.30	0.27	0.63	0.20	1.74	0.322
1300	0.27	0.25	0.62	0.19	1.74	0.305
1400	0.24	0.21	0.56	0.15	1.69	0.278

Next technological structural modification of $MgAl_2O_4$ ceramics was done by increasing sintering duration up to 5 and 9 h while keeping the temperature fixed at 1300 °C and 1400 °C. Results are summarized in Table 2.

Table 2. PALS characteristics for $MgAl_2O_4$ ceramics obtained at T_s = 1300–1400 °C during 2, 5, and 9 h.

T_s, °C/h	τ_1, ns	I_1, a.u.	τ_2, ns	I_2, a.u.	τ_3, ns	I_3, a.u.	τ_{av}, ns	τ_b, ns	κ_d, ns^{-1}	$\tau_2 - \tau_b$, ns	τ_2/τ_b	R_3, nm
1300/2	0.17	0.67	0.40	0.32	2.24	0.01	0.24	0.21	1.0	0.19	1.9	0.309
1300/5	0.16	0.71	0.38	0.28	2.17	0.01	0.22	0.19	1.0	0.19	2.0	0.303
1300/9	0.15	0.74	0.37	0.25	2.38	0.01	0.21	0.18	1.0	0.19	2.1	0.321
1400/2	0.16	0.78	0.38	0.21	2.18	0.01	0.20	0.18	0.9	0.20	2.1	0.304
1400/5	0.15	0.77	0.37	0.22	2.17	0.01	0.20	0.17	0.9	0.20	2.2	0.303
1400/9	0.15	0.77	0.37	0.22	1.83	0.01	0.20	0.17	0.9	0.20	2.2	0.271

As can be concluded from the data of Table 2, lifetimes of the first and the second components (τ_1 and τ_2, respectively) and intensity I_2 decrease with increasing the sintering duration from 2 h to 5 h and 9 h, while intensity I_1 increases following the increase of principle $MgAl_2O_4$ spinel ceramics phase amount. Decrease of I_2 from 0.32 down to 0.25 a.u. with increasing sintering duration from 2 to 9 h in the ceramics that were sintered at 1300 °C is related to the decrease in the amount of free volume defect-related positron trapping centers created due to separated additional phases near grain boundaries. Similar changes

were observed in the case of increased ceramics sintering temperature (see Figure 2). In the ceramics sintered at 1400 °C during 5 and 9 h, lifetimes and intensities of the first and the second components are not changed. This is because the amount of an additional MgO phase is almost the same [42]. The lifetime of the third component at the constant intensity I_3 = 0.01 in the ceramics sintered at 1300 °C increases when the sintering duration is 9 h. This indicates the increase of the size of the nanopore near grain boundaries which might have a negative effect on the functional properties of these ceramics. A schematic depiction of the process is presented in Figure 5.

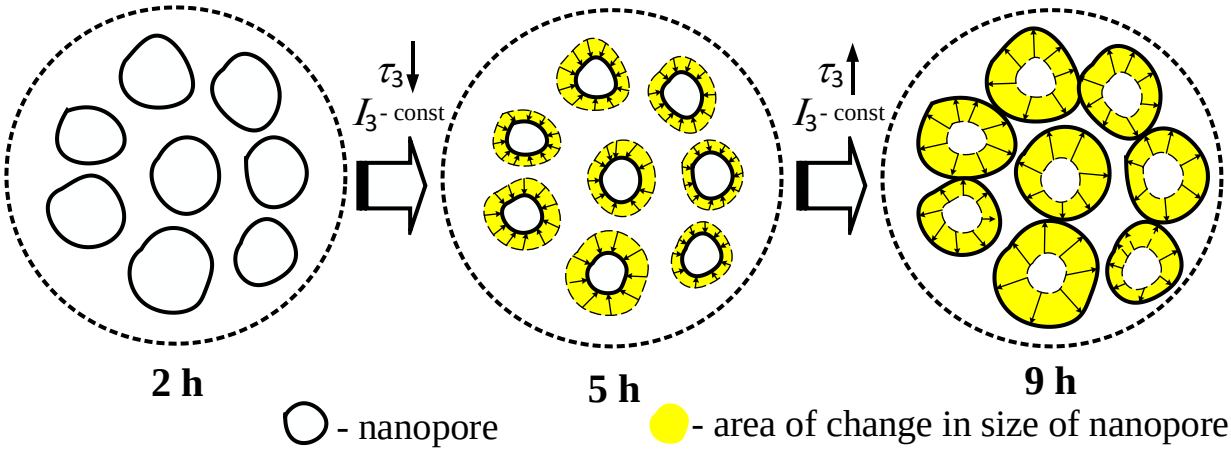

Figure 5. Scheme of nanopores evolution near grain boundaries in $MgAl_2O_4$ ceramics sintered at 1300 °C during 2, 5, and 9 h.

In the ceramics sintered at 1400 °C, lifetime τ_3 is decreased and close to the value that reflects the "pick-off" annihilation of o-Ps in water. It is likely that in such ceramics additional moisture adsorption is possible. Positron trapping parameters as expected to be not significantly different for various ceramics sintering durations (2, 5, and 9 h) at 1300 °C and 1400 °C temperatures.

Additionally, using the lifetime of the third component we can calculate nanopores radii assuming spherical approximation and using the Tao-Eldrup model [49–52]:

$$\tau_{o-Ps} = \left[2\left(1 - \frac{R}{R+\Delta R} + \frac{1}{2\pi} sin\left(\frac{2\pi R}{R+\Delta R}\right)\right) + 0.007\right]^{-1}, \quad (5)$$

where ΔR is empirically obtained parameter ($\Delta R \approx 0.1656$ nm) describing effective electron layer thickness related to the "pick-off" annihilation of o-Ps in an empty space.

Calculation results are provided in Tables 1 and 2 as well as in Figure 6. Nanopores radii calculated based on lifetimes values of the third component for $MgAl_2O_4$ ceramics vary within the range of 0.28–0.34 nm. This can serve as a validation of the fact that the PALS method can also be used to determine nanovoids size in functional materials.

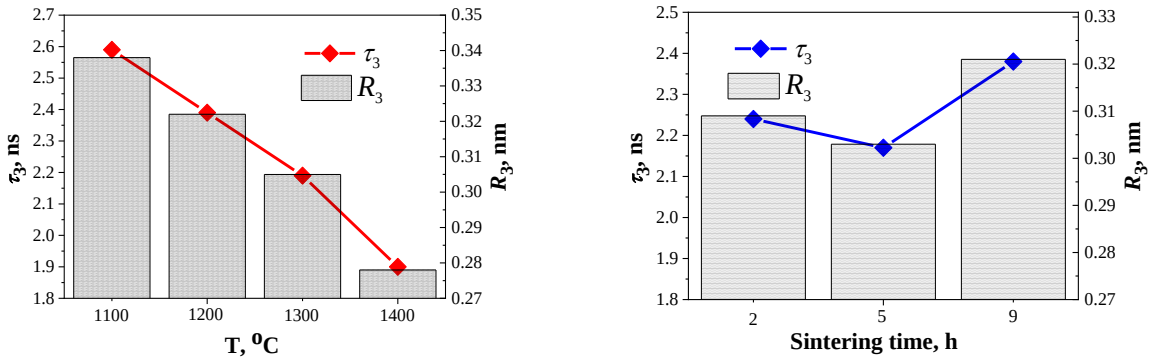

Figure 6. Dependencies of lifetime τ_3 and nanopores radius R_3 calculated according to Tao-Eldrup model for $MgAl_2O_4$ ceramics obtained at 1100–1400 °C and sintering duration of 2 h (**a**) and at 1300 °C and sintering duration 2, 5, and 9 h (**b**).

4. Conclusions

Positron annihilation processes in functional ceramic materials with pronounced porosity (on the example of technologically modified nanostructured $MgAl_2O_4$ ceramics) are described within a two-channel model: positron trapping and o-Ps atoms decay channels. In low statistic measurement mode, better results in PALS analysis are achieved when using three-component decomposition. The first component reflects the main microstructural features of spinel ceramics with tetrahedral and octahedral vacancies, the second one corresponds to the extended free-volume defects (positron trapping sites) localized near grain boundaries and the third component describes the annihilation of o-Ps atoms in nanopores.

Technological conditions of $MgAl_2O_4$ ceramics preparation (maximum temperature and duration of sintering) are the factors that define the annihilation spectra of positron lifetimes. Positron lifetimes of the first and the second components and the intensity of the second component I_2 obtained from investigated PALS spectra decrease, while the intensity of the first component I_1 increases for more perfect ceramics structure with I_3 remaining unchanged. This is evidence of better sintering of ceramic grains accompanied by decreasing defect-related free volume at grain boundaries and nanopores size with an overall amount of nanopores basically unaffected.

Results obtained by PALS can serve as a research background for the development of independent methods of diagnosing nanosized free volumes in ceramic materials, including neutron and heavy-ion irradiated $MgAl_2O_4$ spinels [53–55], Si_3N_4 [56], Ge_3N_4 [57], and AlN [58–60] (which are especially promising as diagnostic materials for EUROfusion applications) and also facilitate understanding of porosity, development, and transformation of pores in electrochemical and other devices for energy conversion [61–68].

Author Contributions: Writing—original draft preparation, H.K.; writing—review and editing, I.K., S.P., and A.I.P.; investigation of ceramics, H.K. and I.K.; treatment of experimental results, H.K. and S.P.; project administration, A.I.P. All authors have read and agreed to the published version of the manuscript.

Funding: H.K. and A.I.P. are grateful for the support from the COST Action CA17126. H.K. was also supported by the Ministry of Education and Science of Ukraine (project for young researchers No. 0119U100435). In addition, I.K. and H.K. were also supported by the National Research Foundation of Ukraine via project 2020.02/0217, while the research of A.I.P. was funded by the Latvian research council via the Latvian National Research Program under the topic "High-Energy Physics and Accelerator Technologies", Agreement No: VPP-IZM-CERN-2020/1-0002. In addition, the research of A.I.P. has been supported by the Latvian-Ukrainian Grant LV-UA/2021/5. The Institute of Solid State Physics, University of Latvia (Latvia) as the Centre of Excellence has received funding from

the European Union's Horizon 2020 Framework Programme H2020-WIDESPREAD01-2016-2017-Teaming Phase2 under grant agreement No. 739508, project CAMART2.

Data Availability Statement: The data presented in this study are available on request from the corresponding author.

Acknowledgments: H.K. and A.I.P. are very grateful to A. Ingram for assistance in experiments and O. Shpotyuk for useful discussion.

Conflicts of Interest: The authors declare no conflict of interest.

References

1. Pethrick, R.A. Positron annihilation—A probe for nanoscale voids and free volume? *Prog. Polym. Sci.* **1997**, *22*, 1–47. [CrossRef]
2. Pereira, V.S.M.; Schut, H.; Sietsma, J. A study of the microstructural stability and defect evolution in an ODS Eurofer steel by means of Electron Microscopy and Positron Annihilation Spectroscopy. *J. Nucl. Mater.* **2020**, *540*, 152398. [CrossRef]
3. Gholami, Y.H.; Yuan, H.; Wilks, M.Q.; Josephson, L.; el Fakhri, G.; Normandin, M.D.; Kuncic, Z. Positron annihilation localization by nanoscale magnetization. *Sci. Rep.* **2020**, *10*, 20262. [CrossRef] [PubMed]
4. Zgardzińska, B.; Chołubek, G.; Jarosz, B.; Wysogląd, K.; Gorgol, M.; Goździuk, M.; Chołubek, M.; Jasińska, B. Studies on healthy and neoplastic tissues using positron annihilation lifetime spectroscopy and focused histopathological imaging. *Sci. Rep.* **2020**, *10*, 11890. [CrossRef]
5. Rementeria, R.; Domínguez-Reyes, R.; Capdevila, C.; Garcia-Mateo, C.; Caballero, F.G. Positron Annihilation Spectroscopy Study of Carbon-Vacancy Interaction in Low-Temperature Bainite. *Sci. Rep.* **2020**, *10*, 487. [CrossRef]
6. Dai, H.; Xie, X.; Chen, Z.; Ye, F.; Li, T.; Yang, Y. Microstructure evolution and magnetic properties of Eu doped CuFeO2 multiferroic ceramics studied by positron annihilation. *Ceram. Int.* **2018**, *44*, 13894–13900. [CrossRef]
7. Bardyshev, I.I.; Gol'danskii, A.V.; Kotenev, V.A.; Tsivadze, A.Y. Positron Annihilation Spectroscopy for the Sintering of Boron Nitride Ceramics. *Prot. Met. Phys. Chem. Surf.* **2018**, *54*, 648–651. [CrossRef]
8. Dai, H.Y.; Liu, H.Z.; Peng, K.; Ye, F.J.; Li, T.; Chen, J.; Chen, Z.P. Correlation between Vacancy Defects and Magnetic Properties of the $GdMn_{1-x}Zn_xO_3$ Multiferroic Ceramics Studied by Positron Annihilation. *Mater. Res. Bull.* **2019**, *119*, 110565. [CrossRef]
9. Mohsen, M.; Gomaa, E.; Al-Kotb, M.S.; Abdel-Baki, M.; Fathy, N. Positron annihilation Lifetime and Fourier transform infrared spectroscopic studies on Bi2O3–B2O3 glasses. *J. Non-Cryst. Solids* **2016**, *436*, 1–8. [CrossRef]
10. Zhao, Y.; Li, D.D.; Qu, B.Y.; Zhou, R.L.; Zhang, B.; Sato, K. Anomalous packing state in Ce-Ga-Cu bulk metallic glasses. *Intermetallics* **2017**, *84*, 25–29. [CrossRef]
11. Li, J.; Wang, G.; Lin, C.; Zhang, T.; Zhang, R.; Huang, Z.; Shen, X.; Gu, B.; Ye, B.; Ying, F.; et al. Free-Volume Defects Investigation of GeS_2-$Ga2S3$-CsI Chalcogenide Glasses by Positron Annihilation Spectroscopy. *Infrared Phys. Technol.* **2017**, *83*, 238–242. [CrossRef]
12. Jean, Y.C.; Van Horn, J.D.; Hung, W.-S.; Lee, K.-R. Perspective of Positron Annihilation Spectroscopy in Polymers. *Macromolecules* **2013**, *46*, 7133–7145. [CrossRef]
13. Sharma, S.K.; Pujari, P.K. Role of free volume characteristics of polymer matrix in bulk physical properties of polymer nanocomposites: A review of positron annihilation lifetime studies. *Prog. Polym. Sci.* **2017**, *75*, 31–47. [CrossRef]
14. James, J.; Thomas, G.V.; Madathil, A.P.; Nambissan, P.M.G.; Kalarikkal, N.; Thomas, S. Positron annihilation spectroscopic characterization of free-volume defects and their correlations with the mechanical and transport properties of SBR–PMMA interpenetrating polymer networks. *Phys. Chem. Chem. Phys.* **2020**, *22*, 18169–18182. [CrossRef]
15. Biswas, D.; Rajan, A.; Kabi, S.; Das, A.S.; Singh, L.S.; Nambissan, P.M.G. Structural defects characterization of silver-phosphate glass nanocomposites by positron annihilation and related experimental studies. *Mater. Charact.* **2019**, *158*, 109928. [CrossRef]
16. Karbovnyk, I.; Collins, J.; Bolesta, I.; Stelmashchuk, A.; Kolkevych, A.; Velupillai, S.; Klym, H.; Fedyshyn, O.; Tymoshuk, S.; Kolych, I. Random nanostructured metallic films for environmental monitoring and optical sensing: Experimental and computational studies. *Nanoscale Res. Lett.* **2015**, *10*, 151. [CrossRef]
17. Kim, S.H.; Chung, J.W.; Kang, T.J.; Kwak, S.-Y.; Suzuki, T. Determination of the glass transition temperature of polymer/layered silicate nanocomposites from positron annihilation lifetime measurements. *Polymer* **2007**, *48*, 4271–4277. [CrossRef]
18. Leipner, H.S.; Hübner, C.G.; Staab, T.E.M.; Haugk, M.; Krause-Rehberg, R. Positron Annihilation at Dislocations and Related Point Defects in Semiconductors. *Phys. Status Solidi* **1999**, *171*, 377–382. [CrossRef]
19. Langhammer, H.T.; Müller, T.; Polity, A.; Felgner, K.-H.; Abicht, H.-P. On the crystal and defect structure of manganese-doped barium titanate ceramics. *Mater. Lett.* **1996**, *26*, 205–210. [CrossRef]
20. Massoud, A.M.; Krause-Rehberg, R.; Langhammer, H.T.; Gebauer, J.; Mohsen, M. Defect Studies in $BaTiO_3$ Ceramics Using Positron Annihilation Spectroscopy. *Mater. Sci. Forum* **2001**, *363–365*, 144–146. [CrossRef]
21. Castro, M.S.; Salgueiro, W.; Somoza, A. Electron paramagnetic resonance and positron annihilation study of the compensation mechanisms in donor-doped ceramics. *J. Phys. Chem. Solids* **2007**, *68*, 1315–1323. [CrossRef]
22. Zhi, Y.; Chen, A. A positron annihilation study of SrTiO3-based ceramics. *J. Physics Condens. Matter* **1993**, *5*, 1877–1882. [CrossRef]
23. Selim, F.A.; Winarski, D.; Varney, C.R.; Tarun, M.C.; Ji, J.; McCluskey, M.D. Generation and characterization of point defects in SrTiO3 and Y3Al5O. *Results Phys.* **2015**, *5*, 28–31. [CrossRef]

24. Banerjee, A.; Sarkar, A.; Sanyal, D.; Chatterjee, P.; Banerjee, D.; Chaudhuri, B.K. Positron annihilation lifetime studies on La0.5Pb0.5Mn1−yCryO. *Solid State Commun.* **2003**, *125*, 65–70. [CrossRef]
25. Hassan, H.E.; Sharshar, T.; Hessien, M.M.; Hemeda, O.M. Effect of γ-rays irradiation on Mn–Ni ferrites: Structure, magnetic properties and positron annihilation studies. *Nucl. Instrum. Methods Phys. Res. Sect. B Beam Interact. Mater. Atoms.* **2013**, *304*, 72–79. [CrossRef]
26. Maheshwari, P.; Keskar, N.; Sudarshan, K.; Manikrishna, K.V.; Krishnan, M.; Pujari, P.K. Investigating defect evolution during thermal treatment in Ni–Cr alloy using positron annihilation spectroscopy. *J. Mater. Sci.* **2020**, *56*, 3498–3509. [CrossRef]
27. Wang, Z.; Dong, X.; Chen, Z.; Xiong, H.; Gao, J.; Du, J.; Tang, X.; Zhang, Q.; Qian, L.; Chen, Z. Dependence of the Ferromagnetism on Vacancy Defect in Annealed In 2 O 3 Nanocrystals: A Positron Annihilation Study. *Phys. Status Solidi* **2021**, *218*. [CrossRef]
28. Ogorodnikova, O.V.; Majerle, M.; Čížek, J.; Simakov, S.; Gann, V.V.; Hruška, P.; Kameník, J.; Pospíšil, J.; Štefánik, M.; Vinš, M. Positron annihilation spectroscopy study of radiation-induced defects in W and Fe irradiated with neutrons with different spectra. *Sci. Rep.* **2020**, *10*, 18898. [CrossRef]
29. Wang, Z.; Yang, Y.; Peng, X.; Huang, Z.; Qian, L.; He, C.; Fang, P. Water diffusivity transition in fumed silica-filled polydimethylsiloxane composite: Correlation with the interfacial free volumes characterized by positron annihilation lifetime spectroscopy. *J. Mater. Sci.* **2021**, *56*, 3095–3110. [CrossRef]
30. El-Shaer, A.; Abdelfatah, M.; Mahmoud, K.R.; Momay, S.; Eraky, M.R. Correlation between photoluminescence and positron annihilation lifetime spectroscopy to characterize defects in calcined MgO nanoparticles as a first step to explain antibacterial activity. *J. Alloys Compd.* **2019**, *817*, 152799. [CrossRef]
31. Ghosh, S.; Nambissan, P.M.G.; Bhattacharya, R. Positron annihilation and Mössbauer spectroscopic studies of In^{3+} substitution effects in bulk and nanocrystalline $MgMn_{0.1}Fe_{1.9-x}In_xO_4$. *Phys. Lett. A* **2004**, *325*, 301–308. [CrossRef]
32. He, J.; Lin, L.-B.; Lu, T.-C.; Wang, P. Effects of electron- and/or gamma-irradiation upon the optical behavior of transparent MgAl2O4 ceramics: Different color centers induced by electron-beam and γ-ray. *Nucl. Instrum. Methods Phys. Res. Sect. B Beam Interact. Mater. Atoms.* **2002**, *191*, 596–599. [CrossRef]
33. Nambissan, P.M.G.; Upadhyay, C.; Verma, H.C. Positron Lifetime Spectroscopic Studies of Nanocrystalline $ZnFe_2O_4$. *J. Appl. Phys.* **2003**, *93*, 6320. [CrossRef]
34. Shantarovich, V.P. Positron annihilation and free volume studies in polymer glasses. *J. Polym. Sci. Part B Polym. Phys.* **2008**, *46*, 2485–2503. [CrossRef]
35. Shpotyuk, O.; Calvez, L.; Petracovschi, E.; Klym, H.; Ingram, A.; Demchenko, P. Thermally-Induced Crystallization Behaviour of $80GeSe_2$–$20Ga_2Se_3$ Glass as Probed by Combined X-Ray Diffraction and PAL Spectroscopy. *J. Alloys Compd.* **2014**, *582*, 323–327. [CrossRef]
36. Klym, H.; Ingram, A.; Shpotyuk, O.; Karbovnyk, I. Influence of CsCl Addition on the Nanostructured Voids and Optical Properties of $80GeS_2$-$20Ga_2S_3$ Glasses. *Opt. Mater.* **2016**, *59*, 39–42. [CrossRef]
37. Klym, H.; Ingram, A.; Shpotyuk, O. Free-Volume Nanostructural Transformation in Crystallized GeS_2-Ga_2S_3-CsCl Glasses. *Mater. und Werkst.* **2016**, *47*, 198–202. [CrossRef]
38. Klym, H.; Ingram, A.; Shpotyuk, O.; Hotra, O.; Popov, A.I. Positron trapping defects in free-volume investigation of Ge–Ga–S–CsCl glasses. *Radiat. Meas.* **2016**, *90*, 117–121. [CrossRef]
39. Klym, H.; Ingram, A.; Shpotyuk, O.; Szatanik, R. Free-Volume Study in GeS_2-Ga_2S_3-CsCl Chalcohalide Glasses Using Positron Annihilation Technique. *Phys. Procedia* **2015**, *76*, 145–148. [CrossRef]
40. Klym, H.; Ingram, A.; Shpotyuk, O.; Hadzaman, I.; Solntsev, V. Water-Vapor Sorption Processes in Nanoporous MgO-Al_2O_3 Ceramics: The PAL Spectroscopy Study. *Nanoscale Res. Lett.* **2016**, *11*, 133. [CrossRef]
41. Filipecki, J.; Ingram, A.; Klym, H.; Shpotyuk, O.; Vakiv, M. Water-sensitive positron trapping modes in nanoporous magnesium aluminate ceramics. *J. Phys. Conf. Ser.* **2007**, *79*, 012015. [CrossRef]
42. Klym, H.; Hadzaman, I.; Shpotyuk, O. Influence of Sintering Temperature on Pore Structure and Electrical Properties of Technologically Modified MgO-Al_2O_3 Ceramics. *Mater. Sci.* **2015**, *21*, 92–95. [CrossRef]
43. Karbovnyk, I.; Bolesta, I.; Rovetskii, I.; Velgosh, S.; Klym, H. Studies of CdI_2-Bi_3 microstructures with optical methods, atomic force microscopy and positron annihilation spectroscopy. *Mater. Sci.* **2014**, *32*, 391–395. [CrossRef]
44. Klym, H.; Ingram, A. Unified model of multichannel positron annihilation in nanoporous magnesium aluminate ceramics. *J. Phys. Conf. Ser.* **2007**, *79*, 012014. [CrossRef]
45. Krause-Rehberg, R.; Leipner, H.S. *Positron Annihilation in Semiconductors: Defect Studies*; Springer: Berlin/Heidelberg, Germany; New York, NY, USA, 1999.
46. Kansy, J.; Giebel, D. Study of defect structure with new software for numerical analysis of PAL spectra. *J. Phys. Conf. Ser.* **2011**, *265*, 012030. [CrossRef]
47. Klym, H.; Lukashevych, D. Multichannel Positron-Positronium Trapping Models for Nanovoids Characterization of Functional Materials. In Proceedings of the 2020 IEEE 40th International Conference on Electronics and Nanotechnology (ELNANO), Kyiv, Ukraine, 22–24 April 2020; pp. 272–275.
48. Dupasquier, A.; De Natale, P.; Rolando, A. Formal calculation of the pick-off annihilation rate for ortho- and parapositronium. *Phys. Rev. B* **1991**, *43*, 10036–10041. [CrossRef]
49. Goworek, T. Comments on the relation: Positronium lifetime–free volume size parameters of the Tao–Eldrup model. *Chem. Phys. Lett.* **2002**, *366*, 184–187. [CrossRef]

50. Zaleski, R.; Wawryszczuk, J.; Goworek, T. Pick-off models in the studies of mesoporous silica MCM-Comparison of various methods of the PAL spectra analysis. *Radiat. Phys. Chem.* **2007**, *76*, 243–247. [CrossRef]
51. Zgardzińska, B. The size of smallest subnanometric voids estimated by positron annihilation method. Correction to the Tao-Eldrup model. *Chem. Phys. Lett.* **2015**, *622*, 20–22. [CrossRef]
52. Gorgol, M.; Maciejewska, M.; Jasińska, B.; Zaleski, R. Testing of the Extended Tao-Eldrup Model on Porous VP-DVB Copolymers. *Mater. Sci. Forum* **2012**, *733*, 24–28. [CrossRef]
53. Seeman, V.; Feldbach, E.; Kärner, T.; Maaroos, A.; Mironova-Ulmane, N.; Popov, A.I.; Shablonin, E.; Vasil'chenko, E.; Lushchik, A. Fast-neutron-induced and as-grown structural defects in magnesium aluminate spinel crystals with different stoichiometry. *Opt. Mater.* **2019**, *91*, 42–49. [CrossRef]
54. Lushchik, A.; Feldbach, E.; Kotomin, E.A.; Kudryavtseva, I.; Kuzovkov, V.N.; Popov, A.I.; Seeman, V.; Shablonin, E. Distinctive features of diffusion-controlled radiation defect recombination in stoichiometric magnesium aluminate spinel single crystals and transparent polycrystalline ceramics. *Sci. Rep.* **2020**, *10*, 7810. [CrossRef]
55. Lushchik, A.; Dolgov, S.; Feldbach, E.; Pareja, R.; Popov, A.I.; Shablonin, E.; Seeman, V. Creation and thermal annealing of structural defects in neutron-irradiated MgAl2O4 single crystals. *Nucl. Instrum. Methods Phys. Res. Sect. B Beam Interact. Mater. Atoms* **2018**, *435*, 31–37. [CrossRef]
56. Feldbach, E.; Museur, L.; Krasnenko, V.; Zerr, A.; Kitaura, M.; Kanaev, A. Defects induced by He+ irradiation in γ-Si_3N_4. *J. Lumin.* **2021**, *237*, 118132. [CrossRef]
57. Feldbach, E.; Zerr, A.; Museur, L.; Kitaura, M.; Manthilake, G.; Tessier, F.; Krasnenko, V.; Kanaev, A. Electronic Band Transitions in γ-Ge_3N_4. *Electron. Mater. Lett.* **2021**, *17*, 315–323. [CrossRef]
58. Kozlovskiy, A.; Kenzhina, I.; Alyamova, Z.; Zdorovets, M.V. Optical and structural properties of AlN ceramics irradiated with heavy ions. *Opt. Mater.* **2019**, *91*, 130–137. [CrossRef]
59. Zdorovets, M.V.; Dukenbayev, K.; Kozlovskiy, A.L. Study of Helium Swelling in Nitride Ceramics at Different Irradiation Temperatures. *Materials* **2019**, *12*, 2415. [CrossRef]
60. Kozlovskiy, A.; Kenzhina, I.; Dukenbayev, K.; Zdorovets, M. Influence of He-ion irradiation of ceramic AlN. *Vacuum* **2019**, *163*, 45–51. [CrossRef]
61. Kurteeva, A.A.; Bogdanovich, N.M.; Bronin, D.I.; Porotnikova, N.M.; Vdovin, G.K.; Pankratov, A.A.; Beresnev, S.M.; Kuz'mina, L.A. Options for adjustment of microstructure and conductivity of cathodic substrates of La(Sr)MnO. *Russ. J. Electrochem.* **2010**, *46*, 811–819. [CrossRef]
62. Porotnikova, N.M.; Eremin, V.A.; Farlenkov, A.S.; Kurumchin, E.K.; Sherstobitova, E.A.; Kochubey, D.I.; Ananyev, M.V. Effect of AO Segregation on Catalytical Activity of $La_{0.7}A_{0.3}MnO_{3\pm\delta}$ (A = Ca, Sr, Ba) Regarding Oxygen Reduction Reaction. *Catal. Lett.* **2018**, *148*, 2839–2847. [CrossRef]
63. Osinkin, D.A.; Khodimchuk, A.V.; Porotnikova, N.M.; Bogdanovich, N.M.; Fetisov, A.V.; Ananyev, M.V. Rate-Determining Steps of Oxygen Surface Exchange Kinetics on $Sr_2Fe_{1.5}Mo_{0.5}O_{6-\delta}$. *Energies* **2020**, *13*, 250. [CrossRef]
64. Suchikova, Y.O. Sulfide Passivation of Indium Phosphide Porous Surfaces. *J. Nano-Electron. Phys.* **2017**, *9*, 1006. [CrossRef]
65. Suchikova, J.A. Synthesis of Indium Nitride Epitaxial Layers on a Substrate of Porous Indium Phosphide. *J. Nano-Electron. Phys.* **2015**, *7*, 03017.
66. Kozlovskiy, A.; Shlimas, D.; Kenzhina, I.; Zdorovets, M. Study of the use of ionizing radiation to improve the efficiency of performance of nickel nanostructures as anodes of lithium-ion batteries. *Mater. Res. Express* **2019**, *6*, 055026. [CrossRef]
67. Rumiantseva, Y.; Melnichuk, I.; Garashchenko, V.; Zaporozhets, O.; Turkevich, V.; Bushlya, V. Influence of cBN content, Al_2O_3 and Si_3N_4 additives and their morphology on microstructure, properties, and wear of PCBN with NbN binder. *Ceram. Int.* **2020**, *46*, 22230–22238. [CrossRef]
68. Olenych, I.B.; Aksimentyeva, O.I.; Monastyrskii, L.S.; Horbenko, Y.Y.; Partyka, M.V. Electrical and Photoelectrical Properties of Reduced Graphene Oxide—Porous Silicon Nanostructures. *Nanoscale Res. Lett.* **2017**, *12*, 272. [CrossRef]